Wind and Structures, Vol. 15, No. 5 (2012) 423-439
DOI: http://dx.doi.org/10.12989/was.2012.15.5.423

Correlation of wind load combinations including torsion on medium-rise buildings

D.C. Keast*[1], A. Barbagallo[2] and G.S. Wood[3]

[1] *Arup Group, Cairns, Australia*
[2] *School of Civil Engineering, The University of Sydney, Australia*
[3] *Cermak Peterka Petersen Pty. Ltd., Australia*

(Received May 16, 2011, Revised November 28, 2011, Accepted December 10, 2011)

Abstract. Three common medium- rise building forms were physically tested to study their overall wind induced structural response. Emphasis was placed on the torsional response and its correlation with other peak responses. A higher correlation was found between the peak responses than between the general fluctuating parts of the signals. This suggests a common mechanism causing the peak event, and that this mechanism is potentially different to the mechanism causing the general load fluctuations. The measurements show that about 80% of the peak overall torsion occur simultaneously with the peak overall along wind drag for some generic building shapes. However, the peak torsional response occurs simultaneously with only 30%-40% of the peak overall drag for the rectangular model. These results emphasise the importance of load combinations for building design, which are often neglected in the design of medium sized rigid buildings for which the along-wind drag is dominant. Current design wind loading standards from around the world were evaluated against the results to establish their adequacy for building design incorporating wind-induced torsion effects. Although torsion is frequently neglected, for some structural systems it may become more important.

Keywords: torsion; wind loading; structural response; medium rise building; correlation; design standards

1. Introduction

Current wind loading standards around the world generally contain little guidance regarding torsional wind loading on building structures. Despite their neglect, torsional loads generated by a continually varying asymmetric pressure distribution around the building can be significant, as discussed by Cheung and Melbourne (2006), Isyumov and Poole (1983), Lythe and Surry (1990), Tamura *et al.* (2001), and Venanzi (2006). Torsional wind loads are often neglected as they are typically small compared with along wind loads, and the natural resistance in rigid structures can resist the loads. As structures become lighter and less rigid, the effect of torsion will become more important for certain structural systems. In portal frame structures the load is resisted by framing action, the asymmetric pressure distribution being resisted by individual portal frames, whereas typical rigid structures resist torsion through material stiffness. Some studies have been completed on the torsional loads on both low and high-rise buildings; for example: Boggs *et al.* (2000),

* Corresponding author, Structural Engineer, E-mail: david.keast@arup.com

Cheung and Melbourne (1992, 2006), Isyumov and Poole (1983), Liang *et al.* (2004), Lythe and Surry (1990), however there has been little experimental data on medium rise buildings, (approximately 8 to 18 stories in height), Tamura *et al.* (2003), which are typical for medium density housing.

Torsional wind loading on buildings is caused by asymmetries in the wind induced pressure distribution. Due to lower magnitudes and generally lower structural importance, torsion is not as well investigated as along-wind (drag) loads, or cross-wind (lift) loads. Methods for estimating wind-induced drag and cross-wind force are well developed for rectangular buildings; however torsion is not as amenable to analytical treatment, (Boggs *et al.* 2000), partly to the fact that structural systems resist the applied pressure distribution differently, and unless asymmetric pressure distributions around the building are defined, overall torsion may not be appropriate. For these reasons, torsional wind loads are not often specified by codes or standards. The neglect of torsional loads arises from the assumption, promoted by some codified models, that the wind loads on a building are uniformly distributed across its faces This rarely proves to be the case as torsional wind loading can be caused by such common factors as turbulence in the flow, the wind acting at an oblique angle to the building face, an asymmetric building form, or non-uniformities in the flow caused by upstream obstructions, (Xie and Gu 2005). The basic, usually conservative, inclusion of torsional wind loading in some codes reflects the complex nature of the problem and highlights the lack of research conducted in this field.

It is commonly known that fluctuations in the along-wind drag are to a large extent generated by the natural turbulence in the approaching flow, but mechanisms causing fluctuations in cross-wind force and torsion are complicated and include the geometry of the body, the relative angle of attack between the body and the wind, natural turbulence, and fluid/body interaction effects such as vortex shedding. Due to the fundamental flow mechanism in the separated zone, it is generally considered that cross-wind force and torsion will be reasonably well correlated, but the drag will not be as well correlated with the other components. Therefore, in the design of rigid mid-rise buildings, the drag response is generally predominant, and the other components and load combinations tend to be neglected. A higher correlation between drag and torsion for peak loading effects on square and rectangular low to medium rise rigid buildings was presented by Tamura *et al.* (2003) for winds normal to the building face, emphasizing the importance of load combinations.

The primary objective of this study was to determine the correlation of wind loading, and whether the current wind loading standards are adequate for practical rigid building design. From papers such as Boggs *et al.* (2000), Lythe and Surry (1990), Tamura *et al.* (2003, 2005, 2007), and Wu and Li (2008), it is evident that the current design codes and standards are inadequate for torsional moment design

2. Experiments

All testing took place in the No.1 boundary layer wind tunnel in the School of Civil Engineering, The University of Sydney. This wind tunnel is an open circuit type wind tunnel with a working section of 2.4 m × 1.8 m and length of 20 m.

Tests were carried out on three separate models, with a length scale of 1:400, chosen to represent common aspect ratios used in medium rise building design. Schematics of the models are shown in Fig. 1. The rectangular model 1 has a similar plan aspect ratio (1 : 2) to that used in the study by Isyumov and

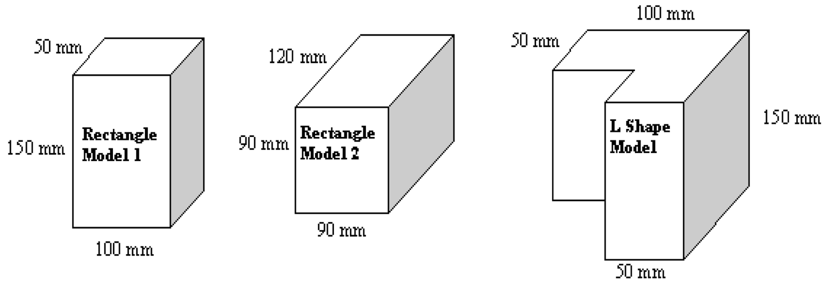

Fig. 1 Schematic of models tested

Poole (1983). These models represent full scale buildings approximately 10 to 18 stories high, depending on floor-to-floor height.

Base shear forces and moments were recorded using a 6 degree-of-freedom high frequency balance for a full-scale equivalent time of 10 hours. Rigid models were tested for a range of wind directions at 15^{o} increments. The natural frequency of the model balance system (over 100 Hz) was high enough that resonant effects were not an issue. The analogue signal was low-pass filtered at 200 Hz, and sampled using a 16 bit A/D system at 400 Hz. Since the prototype buildings are considered rigid the raw data were used directly to determine the peak events. The measured peak events presented herein were calculated as the average of the ten, one hour samples. A predicted peak was also calculated using a crossing analysis (Rofail and Kwok 1992). The probability of exceedence used in the crossing analysis was 0.1%.

Each model was tested in a wind environment simulating open country and suburban terrain as described in Standards Australia (2011). A comparison between the measured and codified profiles is presented in Fig. 2 showing good agreement in accordance with the AWES QAM ±10% error recommendation. Profiles of mean wind speeds were obtained indirectly from AS/NZS1170.2, using the tabulated terrain- height multipliers for gust wind speeds and the listed turbulence intensities.

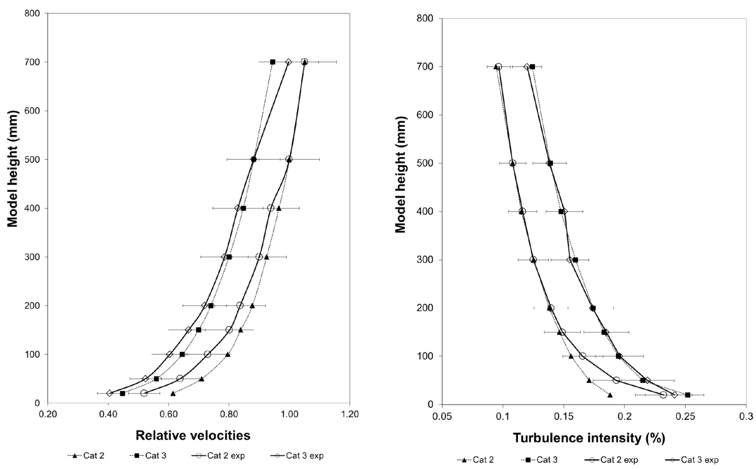

(a) Normalised mean wind speed (b) Turbulence intensity

Fig. 2 Comparison of measured wind velocity profiles with AS/NZS1170.2; error bars shown in accordance with the AWES (2001)

Table 1 Reference dimensions for the model subject buildings in Fig. 1 Schematic of models tested

Dimension	Rectangular model 1	Rectangular model 2	*L*-shaped model
b/mm	100	120	100
h/mm	150	90	150

The turbulence intensity for the case of Terrain Category 2 in Fig. 2 is closer to a Terrain Category 2.5 in approximately the lower half of the height of the model and is within the AWES (2001) ±10% error recommendation except near the base of the model where the wind loads are significantly smaller.

For convenience, the recorded base forces and moments: along-wind (drag) shear force, *D*; cross-wind (lift) shear force, *L*; and torsional moment, *T* are presented in coefficient form.

$$C_D = \frac{D}{\frac{1}{2}\rho \cdot \overline{V}_h^2 \cdot b \cdot h} \tag{1}$$

$$C_L = \frac{L}{\frac{1}{2}\rho \cdot \overline{V}_h^2 \cdot b \cdot h} \tag{2}$$

$$C_T = \frac{T}{\frac{1}{2}\rho \cdot \overline{V}_h^2 \cdot b \cdot h} \tag{3}$$

where $\frac{1}{2}\rho \cdot \overline{V}_h^2$ is the mean dynamic wind pressure acting on the building at roof height, $\overline{V}_h$, is the mean wind speed at roof height, *b* is the longest plan form dimension for the building, and *h* is the building height, Table 1.

3. Results

The wind axis notation used to describe the wind loading is shown in Fig. 3. The mean torsion for rectangular model 1 is presented in Fig. 4 alongside the results of Isyumov and Poole (1983), which were conducted on a model with the same plan form aspect ratio. This figure shows excellent similarity between studies.

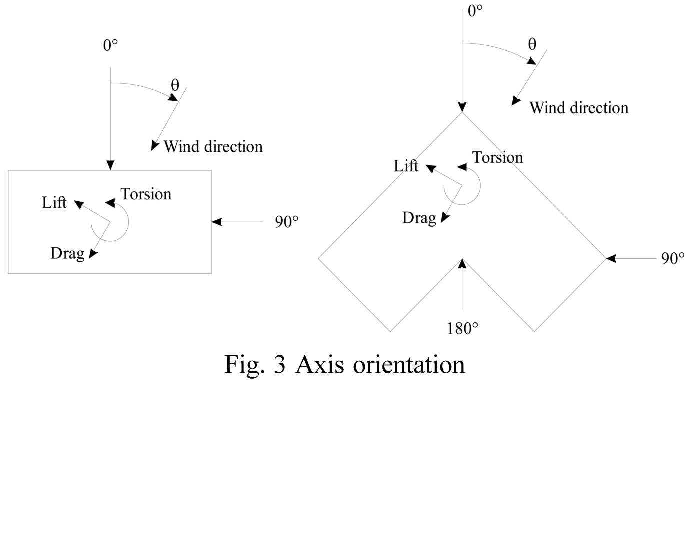

Fig. 3 Axis orientation

Fig. 4 to Fig. 6 show the force and moment coefficients C_T, C_D, and C_L, with azimuth for the rectangle model 1 tested in open country terrain conditions. These graphs show mean, measured peaks, and predicted peaks, identified using the 'pred' subscript, using the crossing analysis of each load effect coefficient. The results for the open country terrain are discussed herein, instead of the suburban terrain results, as they showed slightly higher correlations in the simultaneous peak responses due to the lower turbulence in the incident flow.

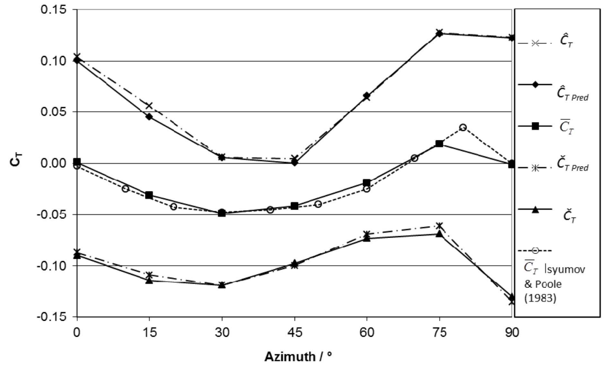

Fig. 4 Torsion coefficient for rectangular model 1, open country terrain

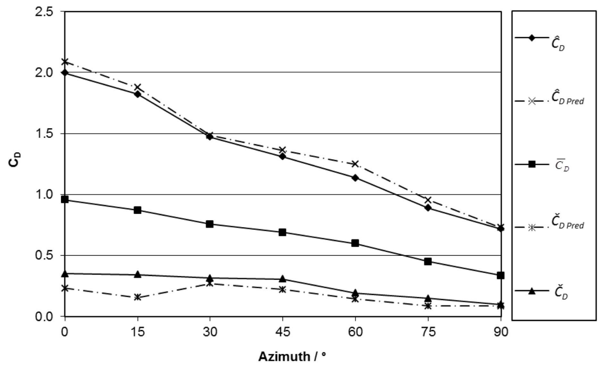

Fig. 5 Drag coefficient for rectangular model 1, open country terrain

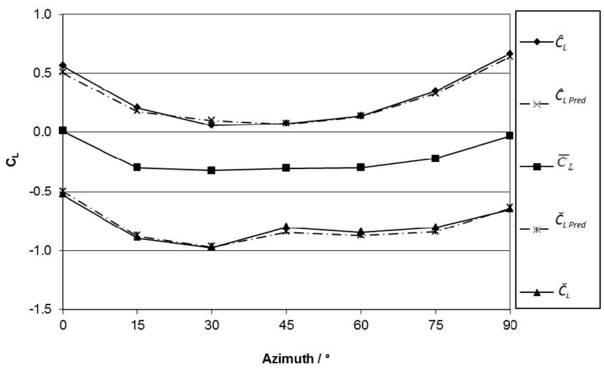

Fig. 6 Cross-wind force coefficient for rectangular model 1, open country terrain

From inspection of Fig. 4 to 6, it is evident that the largest forces and moments (i.e., torsion, drag, and cross-wind force) do not occur for the same incident wind angle. There is good similarity between the measured and predicted peaks using the crossing analysis, validating the applicability of using a crossing analysis to predict the peak event in this situation.

The maximum magnitude of mean base torsion coefficient occur at azimuth angles of 30° and 75°, Fig. 4. As expected the drag coefficient C_D decreases with azimuth as is evident in Fig. 5. The mean cross-wind force coefficient, $\overline{C}_L$, Fig. 6, shows the expected value of zero when the wind is normal to a building face, 0° and 90°. The maximum values of the mean cross-wind force coefficient $\overline{C}_L$ are achieved for a wide range of azimuths from about 15° to 60°.

It is important to distinguish the mechanism causing the mean torsion from the peak torsion. Mean torsion is based on a mean pressure distribution around the building. From quasi-steady theory, the peak torsion would be caused by the same mechanism causing the mean torsion. However, a different mechanism from the mean pressure distribution, such as an extreme vortex at the leading edge or flow reattachment could cause the peak event. Although difficult to distinguish mechanisms from a base balance compared with a simultaneous pressure test, a crossing analysis can indicate mixed mechanisms. The results of the crossing analysis for the rectangular model 1 in open country terrain at an azimuth of 75° and at 90° are shown in Fig. 7. Both azimuths show results that are close to Gaussian for the main body of the results; however the results for 75° indicate the signal is slightly more random than at 90°; depicted by a lower gradient. The higher level of randomness suggests that a more intermittent mechanism, such as higher intensity vortices at the leading edge, is causing the peak torsion events. This is also indicated by the flattening of the up-crossing line towards the extreme event indicating that large peak events have occurred. To investigate this further, pressure distribution information would be required, which was outside the scope of this study.

For the L shape model, the mean torsion coefficient, $\overline{C}_T$, reaches a peak negative value at 60°, Fig. 8. It was evident from the results that the fluctuating component of torsion changed significantly with azimuth, with the highest component at 45° when the wind is normal to the wide face of the L, Fig. 3. The mean drag coefficient, $\overline{C}_D$, reaches a maximum value at an azimuth of 180°, where the wind is blowing directly into the recess of the L. A localised maximum value occurs at an azimuth of 45°, Fig. 9, where the wind is perpendicular to the wide face of the L shape. The peak drag coefficient, $\hat{C}_D$, reaches a maximum value at 150°, with a plateau of similar values

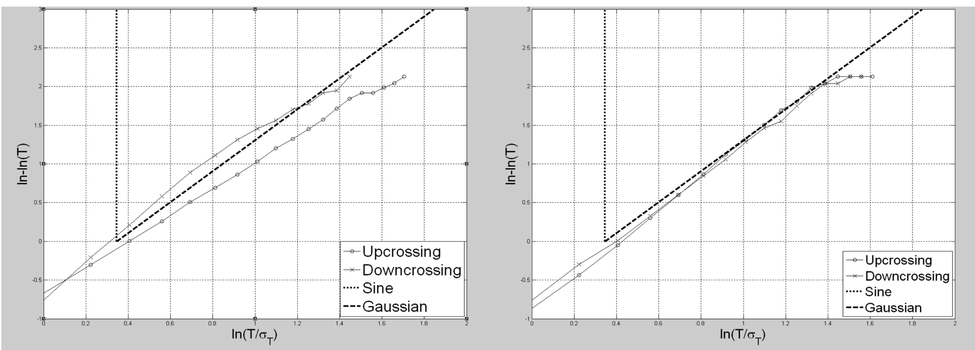

(a) (b)

Fig. 7 Crossing peak torsion distribution for rectangular model 1 in open country terrain

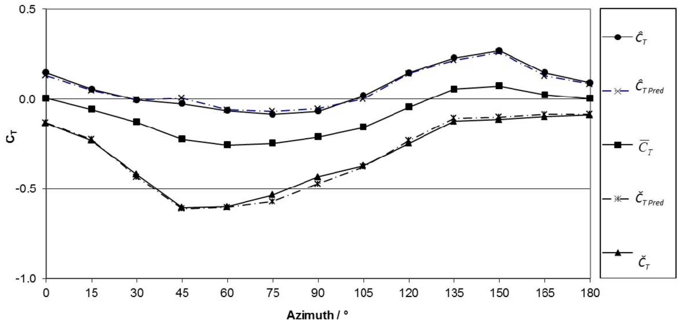

Fig. 8 Torsion coefficient for *L* shaped model, open country terrain

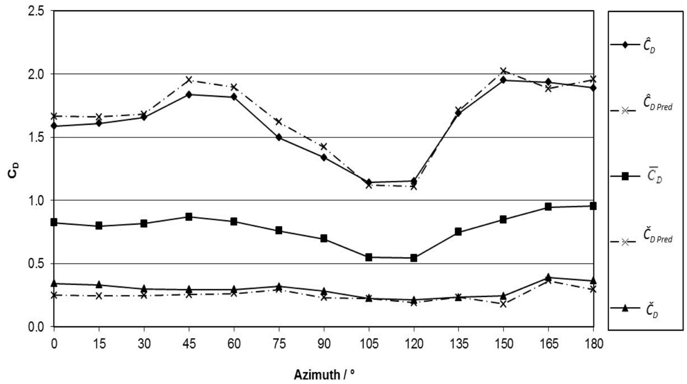

Fig. 9 Drag coefficient for *L* shaped model, open country terrain

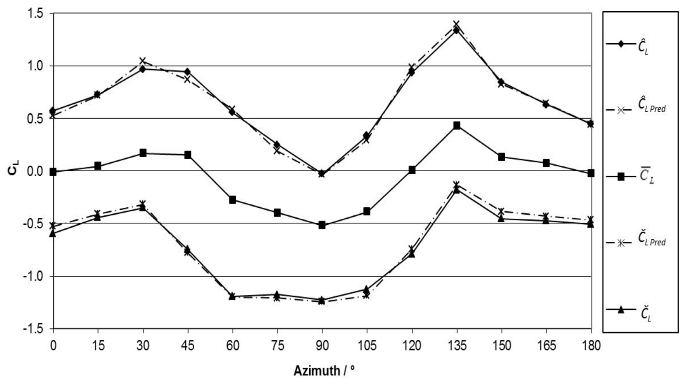

Fig. 10 Cross-wind force coefficient for *L* shaped model, open country terrain

to 180º. The maximum value of mean cross-wind coefficient, $\overline{C}_L$, Fig. 10, occurred at an azimuth of 90º and 135º caused by the asymmetric wake formed by separation at the leading edges. The fluctuating component of cross-wind force is similar for all wind directions.

Fig. 11 to Fig. 13 show examples of phase-plane expressions of wind load combinations. The records correspond to 10 hours in prototype scale. Fig. 11(a) to Fig. 13(a) and Fig. 11(b) to Fig. 13(b) show rectangular model 1 in open country terrain and suburban terrain respectively at the same wind direction. Fig. 11(c) to Fig. 13(c) shows the *L* shape model in open country terrain. These are

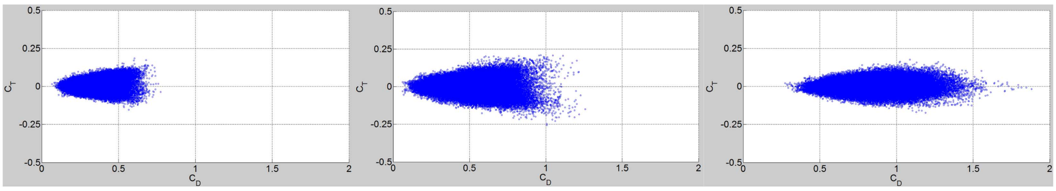

(a) (b) (c)

Fig. 11 Phase-plane expressions of wind load combinations C_D-C_T for: (a) the rectangular model 1 in open country terrain at an azimuth of 90º, (b) the rectangular model 1 in suburban terrain at an azimuth of 90º and (c) the *L* shape model in open country terrain at an azimuth of 0º

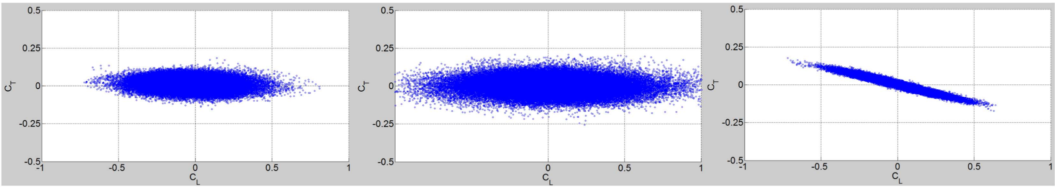

(a) (b) (c)

Fig. 12 Phase-plane expressions of wind load combinations C_L-C_T for (a) the rectangular model 1 in open country terrain at an azimuth of 90º, (b) the rectangular model 1 in suburban terrain at an azimuth of 90º and (c) the *L* shaped model in open country terrain at an azimuth of 0º

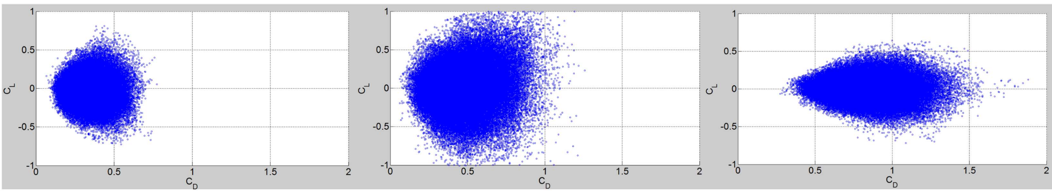

(a) (b) (c)

Fig. 13 Phase-plane expressions of wind load combinations C_D-C_L for (a) the rectangular model 1 in open country terrain at an azimuth of 90º, (b) the rectangular model 1 in suburban terrain at an azimuth of 90º and (c) the *L* shaped model in open country terrain at an azimuth of 0º

representative figures and are indicative for a number of wind directions.

As expected there was a wider scatter observed for the suburban terrain data, Fig. 11(b) to Fig. 13(b), implying higher turbulence buffeting and reduced correlation between the loading effects when compared with the open country terrain results, Fig. 11(a) to Fig. 13(a). Suburban terrain generates lower simultaneous loadings, and the results presented here focus on the open country terrain results.

The combinations of drag and torsion coefficient, C_D-C_T, in Fig. 11 show wedge shaped loci expanding from near the origin. From these wedge shaped loci it is evident that the base torsion coefficient C_T can take any value when the drag force coefficient C_D records its peak; thus the peaks could occur near simultaneously. This broad correlation indicates that there is not a simple relationship between the two responses and a number of different mechanisms are present. Away from these azimuths, the loci become skewed and asymmetric indicating a more complex relationship between the drag and torsion responses.

The relationship between cross-wind force and torsion, C_L-C_T, Fig. 12, and drag and cross-wind force C_D-C_L, Fig. 13, shows elliptic loci, with little correlation at the peak events.

4. Combinations of quasi-steady loads

For each of the ten 1-hour full scale equivalent runs, the peak value of one of the loads, i.e., peak torsion, drag, or cross-wind force coefficient was selected and the other simultaneous loads were determined from the time series. When the peak torsion coefficient $\hat{C}_T$ occurs these are indicated as $C_D(\hat{C}_T)$ and $C_L(\hat{C}_T)$. The other combinations $[C_T(\hat{C}_D)$ and $C_L(\hat{C}_D)]$ and $[C_T(\hat{C}_L)$ and $C_D(\hat{C}_L)]$ were also captured when the peak drag coefficient $\hat{C}_D$, and the peak cross-wind force coefficient $\hat{C}_L$, respectively, were recorded. Henceforth the peak load effects $\hat{C}$ are actually the largest absolute value of the measured peak load effects $\hat{C}$ and $\check{C}$. This has particular implications for cross-wind forces and torsion, as it is not important which way the building is twisting or being loaded respectively (although it may be of importance depending on the adopted structural system). The peak drag coefficients are always positive, so taking the absolute value has no effect.

For the rectangular model 1 in open country terrain, Fig. 14(a) shows the combination of peak drag coefficient $\hat{C}_D$ and the ratio of simultaneously recorded torsional base moment coefficient $C_T(\hat{C}_D)/\hat{C}_T$, which is the ratio of the simultaneously recorded torsional base moment coefficient $C_T(\hat{C}_D)$ to its maximum value $\hat{C}_T$ for each 1-hour run. Fig. 14(b) shows the ratio of simultaneously recorded torsional base moment coefficient $C_T(\hat{C}_D)/\hat{C}_{T_{overall}}$, which is the ratio of the simultaneously recorded torsional base moment coefficient $C_T(\hat{C}_D)$ to the maximum of the peak torsional base moment coefficients $\hat{C}_T$ recorded for the ten 1-hour runs for all the angles of wind incidence. Fig. 14(b) is

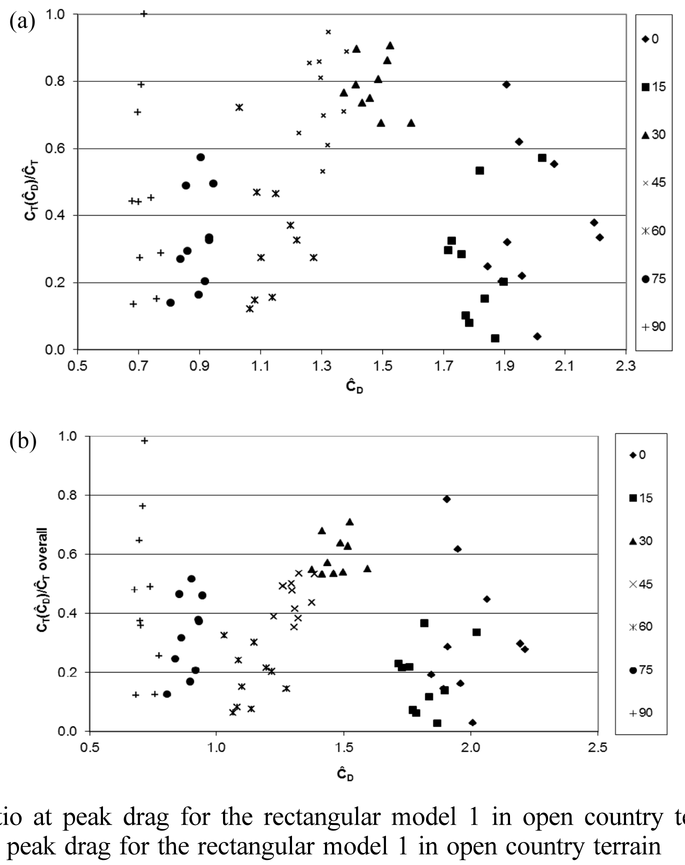

Fig. 14 (a) Torsion ratio at peak drag for the rectangular model 1 in open country terrain and (b) overall torsion ratio at peak drag for the rectangular model 1 in open country terrain

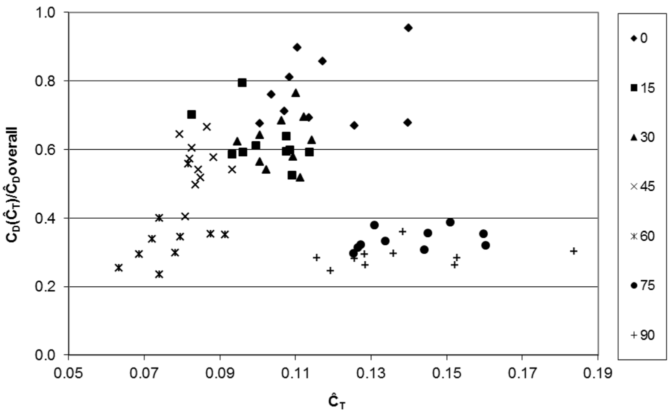

Fig. 15 Overall drag ratio at peak torsion for the rectangular model 1 in open country terrain

considered more appropriate from a design and codification perspective, for which consideration of specific wind data from all angles is not necessarily appropriate, and a simplified approach using a more generalised tool is necessary. Fig. 14(a) is more useful from a theoretical perspective where identifying the mechanisms causing the torsion may be of importance.

When the peak drag $\hat{C}_D$ occurs at a specific wind direction, Fig. 14(a), 0-80% of the peak torsion $\hat{C}_T$ was simultaneously recorded. The highest ratio of simultaneously recorded torsion occurred at an angle of wind incidence of 30° which exhibits 70-90% of the peak torsion for these runs. Although an angle of wind incidence of 30° exhibits a fairly high mean base torsion coefficient, $\overline{C}_T$, as shown in Fig. 4, it does not exhibit the maximum peak base torsion coefficient $\hat{C}_T$, which occurs at 75°. So even though the highest ratio of simultaneously recorded torsion occurs at this angle, the peak torsion is reduced from the overall peak torsion experienced by the building for all angles of wind incidence.

Fig. 15 shows the relationship between peak base torsion coefficient $\hat{C}_T$ and the ratio of simultaneously recorded drag coefficient $C_D(\hat{C}_T)/\hat{C}_{D_{overall}}$. When the maximum values of peak base torsion coefficient $\hat{C}_T$ occur, at an azimuth of 75°, 30-40% of the maximum peak drag occurs simultaneously. The peak torsions at azimuths 75° and 90° are similar. This tends to suggest that the peak base torsion events are caused by winds from a direction slightly skewed to the building axis of symmetry, reinforcing the work of Boggs *et al.* (2000). These similar distributions also suggest that the mechanism causing the peak torsion may be similar to that causing the mean torsion. A single outlying point for high base torsion is recorded at an azimuth of 90°; although this point is the highest recorded peak torsion it is an outlier with respect to the distribution for all 10 peak values at 90°. For this reason, as well as the fact that at 75° exhibits a higher mean of the peak drags recorded and higher simultaneous drag coefficients, 75° is considered more important.

The combinations of peak cross-wind force coefficient and peak torsion coefficient, with their respective simultaneous load effects for the rectangular model 1 in open country terrain, are shown in Figs. 16 and 17 respectively. Almost 90% of the peak overall base torsion coefficient is observed when the peak cross-wind force coefficient is observed. When the maximum of the peak torsion coefficients $\hat{C}_T$ occurs, evident at an azimuth of 75°, 0-20% of the peak overall cross-wind force coefficient occurs simultaneously. This is lower than the simultaneous drag coefficient $C_D(\hat{C}_T)/\hat{C}_{D_{overall}}$ observed as discussed in the previous paragraph. These results suggest that there is a higher correlation between the peak drag coefficients $\hat{C}_D$ and the peak torsion coefficients $\hat{C}_T$ than that

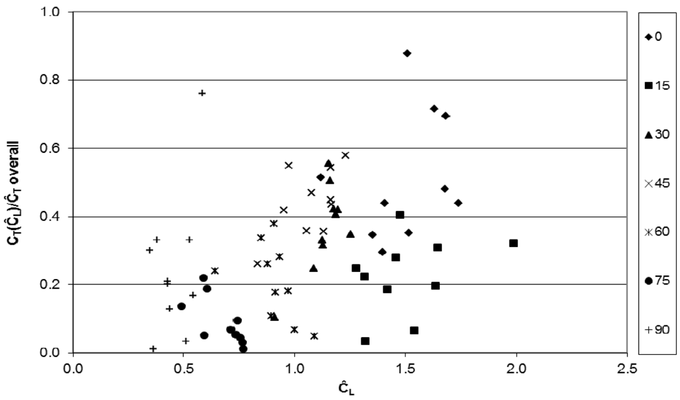

Fig. 16 Overall torsion ratio at peak cross-wind force for the rectangular model 1 in open country terrain

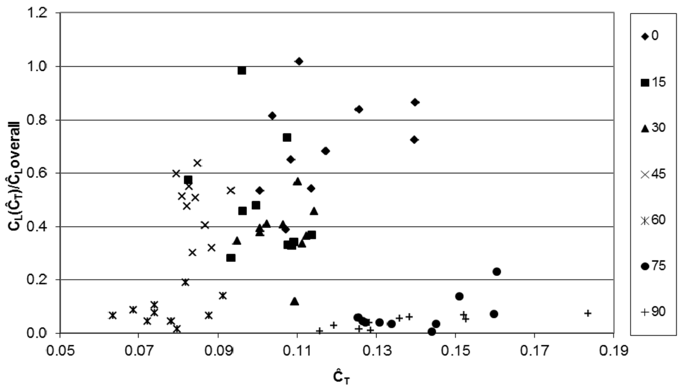

Fig. 17 Overall cross-wind force ratio at peak torsion for the rectangular model 1 in open country terrain

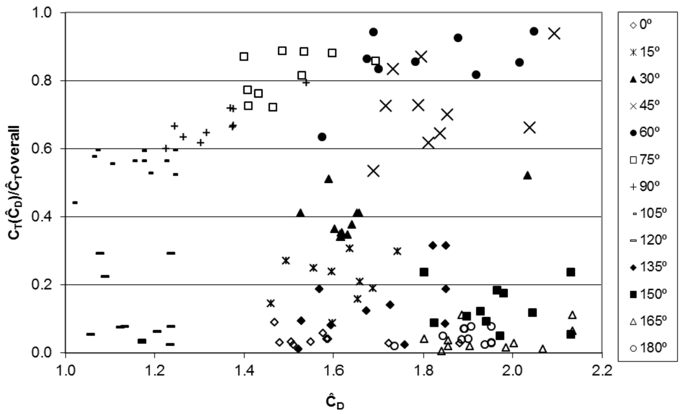

Fig. 18 Overall torsion ratio at peak drag for the L shaped model in open country terrain

between the peak cross-wind force coefficients $\hat{C}_L$ and the peak torsion coefficients $\hat{C}_T$, and that therefore the design case for medium rise rectangular buildings will be generally governed by the drag-torsion relationship. Similar findings were recorded for rectangle model 2.

For the *L* shape building in open country terrain, Fig. 18 shows the overall torsion ratio at peak

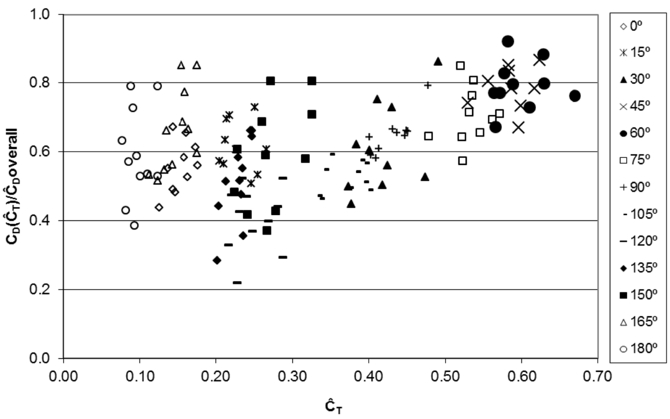

Fig. 19 Overall drag ratio at peak torsion for the L shaped model in open country terrain

drag. The largest peak drag coefficients occur at azimuths about 45° and 150°, where > 70% and < 30% of the peak torsion coefficient is recorded simultaneously. Fig. 19 shows the overall drag ratio at peak torsion, which is approximately three times that of the rectangular model 1. Of interest is the agreement between the points, suggesting a common mechanism causing the peak torsion and large simultaneous drag responses. The largest peak torsion is recorded at an azimuth of 60°, where a drag coefficient of 70-90% of the largest peak drag is simultaneously recorded. Similarly to the rectangular models, the overall magnitude of the cross-wind force is smaller than the drag and there is less correlation between peak cross-wind forces and torsion than peak drags and torsions, reinforcing the belief that the drag-torsion relationship will usually be the design case for medium rise design.

For Fig. 14 to Fig. 19 there is a spread in the peak loads for each of the 10 sub-runs. For the purposes of this study the range is considered to represent the design points, not the highest peak load of the 10 sub-runs, as this would have a different probability of occurrence.

5. Predictions of peak wind load events

For structural design it is important to have a means of estimating design loading effects. The statistics of the wind time series are of interest as these can be used to predict the peak events, rather than using the actual time series that change for each run.

The difficulty with wind being a random process is that the peak structural response within an averaging period is a random variable. Using the assumption that the response distribution is Gaussian, a predicted peak value within an averaging period can be estimated. Using drag as an example, the relationship between peak and mean is expressed by

$$\hat{C}_{DPred} = \overline{C}_D + g_f \sigma_D \tag{4}$$

where

$\hat{C}_{DPred}$ is the predicted peak drag coefficient for a particular time interval,

$\overline{C}_D$ is the mean drag coefficient for the time interval,

g_f is a peak factor for Gaussian approximation, which for the purposes of this paper has been taken as 4, the upper end of the Gaussian range, and

σ_D is the standard deviation of the drag time series.

The correlation between C_D-C_T was calculated and used to predict the torsion that occurs simultaneously with the peak drag following the equation

$$C_T(\hat{C}_D)_{predicted} = \bar{C}_T \pm C_{DT} g_f \sigma_T \tag{5}$$

Where

$C_T(\hat{C}_D)_{predicted}$ is the expected predicted torsion coefficient which occurs simultaneously with the peak drag coefficient.

$\bar{C}_T$ is the average torsion coefficient calculated for each 1 hour sub-run.

C_{DT} is the average correlation between torsion and drag coefficients calculated for each 1 hour sub-run.

σ_T is the average standard deviation of the torsion time signal, calculated for each sub run.

This was similarly conducted for C_L-C_T relationship.

Fig. 20 shows a comparison of the measured and predicted peak drag coefficients and simultaneous torsion coefficient ratios, normalised against the experimental peak torsion values to show what ratio of the experimental peak torsion values occur simultaneously with the peak drag, for rectangular model 1 and the *L*-shaped model at directions producing the maximum peak drag coefficient in open country terrain. The predicted peak drag coefficients $\hat{C}_{D_{pred}}$ are similar to the experimental values $\hat{C}_D$. However, the predicted simultaneous torsion coefficients $C_T(\hat{C}_D)_{pred}$ are typically underestimated for the rectangular model 1, although the spread in data is large. This may be a function of the selection of peak factor for Eq. (5) and the assumption that the mean correlation applies to the peak event, however this implies that the peak drag coefficient $\hat{C}_D$ typically has a higher correlation to the torsion coefficient C_T than that of the general fluctuating part of the time series. This implies that the mechanism causing the peak events differs from the mechanism causing the general events. The spread in data suggests there are a number of potential mechanisms occurring at the peak event, however the pressure distributions around the building would be required to confirm this fully. The predicted and experimental values for the *L*-shaped model in open country terrain show the predictions are close

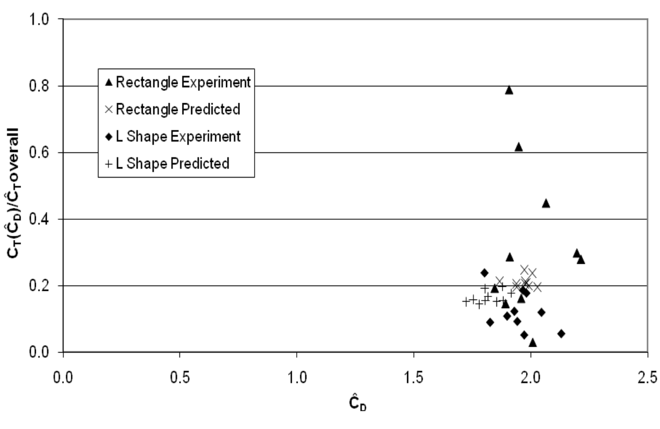

Fig. 20 Measured and predicted peak drag coefficient and simultaneous torsion coefficient ratio $C_T(\hat{C}_D)$ for rectangular model 1 and *L* shape model, at the maximum peak drag, 0° and 150°, in open country terrain

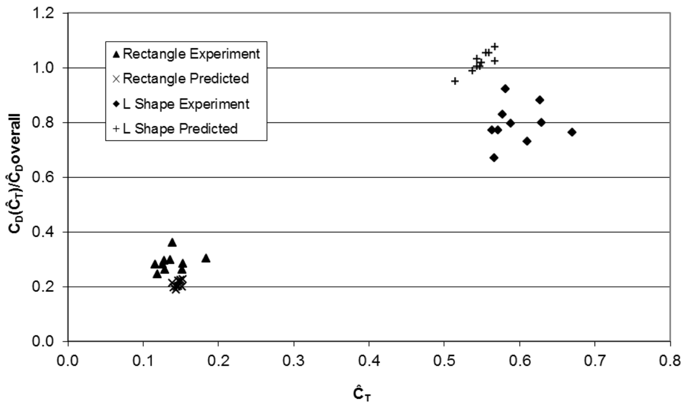

Fig. 21 Measured and predicted peak torsion coefficient and simultaneous drag coefficient $C_D(\hat{C}_T)$ for rectangular model 1 and L shape model, at maximum peak torsion, 90º and 60º, in open country terrain

to experimental results.

A comparison between the measured and predicted peak torsion coefficients, $\hat{C}_{T_{pred}}$, and the simultaneous drag force are shown in Fig. 21. The predicted peak torsion coefficients are similar to the experimental values, $\hat{C}_T$, for the rectangle model 1. The predicted simultaneous drag coefficients, $C_D(\hat{C}_T)_{pred}$, underestimate the experimental simultaneous drag coefficients $C_D(\hat{C}_T)$ by about 10-20%.

These findings contradict the belief that the peak torsional response would coincide with the peak cross-wind force and not the peak drag force. These findings reinforce the work of Tamura *et al.* (2000, 2001, 2003) who found a higher correlation between drag and torsion for peak events for a low-rise, square plan form building.

Although the peak torsion coefficient $\hat{C}_T$ is slightly under estimated when compared to the experimental value for the L-shaped model, the predictions of the simultaneous drag coefficients $C_D(\hat{C}_T)_{pred}$ are conservative by 20-30%. The predictions are less accurate for the L shape model than for the rectangle model 1, suggesting that the mechanism causing the peak events is not similar to the general mechanism. This is possibly because the mechanism causing the large peaks for the rectangle model 1 is suppressed with the L shape. It is not possible to identify the particular mechanisms causing the peaks using the base balance technique used in this investigation, but could be done with a simultaneous pressure experiment.

6. Design standards

Three wind load provisions were chosen for comparison with the wind tunnel data: ASCE 7 (American Society of Civil Engineers 2010), ISO 4354 (International Standards Organisation 2009), and AS/NZS 1170.2:2011 (Standards Australia 2011). Although the standards do not specifically cater for the L shaped geometry, an engineering interpretation of the standards was used to estimate the peak torsion.

ASCE 7 (2010), which is similar to the National Building Code of Canada, is the only standard studied that incorporates torsion for medium-rise buildings. It compares two separate load cases:

75% of the peak along wind drag applied at 15% eccentricity of the windward wall and; 56.3% of the peak along wind drag at 15% eccentricity simultaneously applied to two adjacent faces. These load cases attempt to consider realistic simultaneous loading effects. Limitations exist in these models, as application of the peak along-wind force at an eccentricity is not appropriate for portal frame design, or buildings with large planform aspect ratios. The rule for torsion in ISO 4354 (2009) is similar to the AIJ Recommendations (Architectural Institute of Japan 2004), and has an intensive method including the calculation of a number of parameters to take into account dynamic torsion effects of tall buildings as well as quasi-static effects. AS/NZS 1170.2:2011 (Standards Australia 2011) contains a clause (Clause 2.5.4) stating that for buildings greater than 70 m tall, torsion should be determined by applying the peak along wind drag at an eccentricity of 20% of the widest face. This comparison is used despite these buildings being shorter than 70 m at prototype scale.

A comparison between the peak torsion predicted by the various standards, and that measured in the wind tunnel, is presented in Table 2. The wind tunnel results are the average of the ten time series sub-runs peak values. It is evident that ASCE 7 (2010) does well at predicting the peak torsion for the rectangular plan form buildings, whilst ISO 4354 and the clause in AS/NZS 1170.2:2011 significantly overestimate the peak torsion coefficient $\hat{C}_T$ for medium-sized buildings.

Suggested load cases for the rectangular and L shape models based on the experimental results are presented in Tables 3 and 4 respectively. For the rectangular models the peak torsion is equivalent to the peak drag applied at an eccentricity of 8% of the widest building face.

Although some interesting results regarding over / under design have been established with these comparisons, an insufficient number of models have been tested to justify any changes to current practice, at this time.

Table 2 Comparison of peak torsion coefficient $\hat{C}_T$, in open country terrain

Model	Standards			Wind Tunnel
	ASCE	ISO	AS/NZS	
Rectangular Model 1	0.13	0.38	0.20	0.14
L Shaped Model	0.13	0.38	0.20	0.60
Rectangular Model 2	0.14	0.48	0.35	0.12

Table 3 Suggested design load combinations for the rectangular models

	Drag	Cross-wind	Torsion
Drag	1	0.5	0.8
Cross-wind	0.9	1	0.6
Torsion	0.4	0.4	1

Table 4 Suggested design load combinations for the *L* shaped model

	Drag	Cross-wind	Torsion
Drag	1	0.55	0.3
Cross-wind	0.95	1	0.35
Torsion	0.9	0.8	1

7. Conclusions

The rigid high frequency balance experimental technique provides an efficient method of testing when investigating the overall quasi-steady load combinations on medium rise rigid buildings. The peak overall torsion for the rectangular models was equivalent to the peak overall drag force applied at an eccentricity of 8% of the widest face. As much as 80% of the peak overall torsion was shown to occur simultaneously as the peak overall drag for some generic building shapes. For the rectangular models the peak torsion occurs simultaneous with 30-40% of the peak overall drag. Although this load case is often neglected, for some structural systems it may become more important.

For peak events at certain wind directions, there is a high correlation between drag and torsion. This is in contrast to the general fluctuating part of the signal, where torsion generally exhibits a low correlation with drag, and a higher correlation with cross-wind force as it is mostly generated by the vortex shedding process. These quasi-static load effects show the limitation of using a Gaussian approximation to predict extreme wind load combinations. These findings suggest an alternative mechanism causing the peak load combinations, reinforcing the findings of Tamura *et al.* (2003).

Different standards were compared with the wind tunnel data for the torsional wind load design of the building models examined. ISO and Standards Australia overestimate the peak torsion by as much as double, whilst ASCE provides a reliable approximation. Although specific evaluations are made of the proposed clause for AS/NZS for the models tested, a much larger range of testing would be needed to justify any reduction in the peak torsion coefficient $\hat{C}_T$ or the load combination effects used for design.

References

American Society of Civil Engineers (2010), ASCE Standard, Minimum Design Loads for Buildings and Other Structures. ASCE 7-10, ASCE, New York, USA.

Architectural Institute of Japan (2004), AIJ recommendations for loads on buildings.

Australian Wind Engineering Society (2001), AWES-QAM-1-2001, Wind Engineering Studies of Buildings.

Boggs, D.W., Hosoya, N. and Cochran, L. (2000), "Sources of torsional wind loading on tall buildings-lessons from the wind tunnel", *Proceedings of the 2000 Structures Congress & Exposition*, Philadelphia, May.

Cheung, J.C.K. and Melbourne, W.H. (2006), "Torsional moments of tall buildings with various planform shapes", *Proceedings of the 12th Australasian Wind Engineering Society Workshop*, Queenstown, February.

Cheung, J.C.K. and Melbourne, W.H. (1992), "Torsional moments of tall buildings", *J. Wind Eng. Ind. Aerod.*, **41-44**, 1125-1126.

International Standards Organisation (2009), Wind Actions on Structures ISO 4354.

Isyumov, N. and Poole, M. (1983), "Wind induced torque on square and rectangular building shapes", *J. Wind Eng. Ind. Aerod.*, **13**(1-3), 183-196.

Liang, S., Li, Q.S., Liu, S., Zhang, L. and Gu, M. (2004), "Torsional dynamic wind loads on rectangular tall buildings", *Eng. Struct.*, **26**(1), 129-137.

Lythe, G.R. and Surry, D. (1990), "Wind-induced torsional loads on tall buildings", *J. Wind Eng. Ind. Aerod.*, **36**(1), 225-234.

Rofail, A.W. and Kwok, K.C.S. (1992), "A reliability study of wind tunnel results for cladding pressure", *J. Wind Eng. Ind. Aerod.*, **44**(1-3), 2413-2424.

Standards Australia (2011), *Structural Design Actions Part 2 Wind Actions*, AS/NZS 1170.2-2011, Standards Australia.

Tamura, Y., Kikuchi, H. and Hibi, K. (2000), "Wind load combinations and extreme pressure distributions on low-rise buildings", *Wind Struct*., **3**(4), 279-289.

Tamura, Y., Kikuchi, H. and Hibi, K. (2001), "Extreme wind pressure distributions on low-rise building models", *J. Wind Eng. Ind. Aerod.*, **89**(14-15), 1635-1646.

Tamura, Y., Kikuchi, H. and Hibi, K. (2003), "Quasi-static wind load combinations for low- and middle-rise buildings", *J. Wind Eng. Ind. Aerod.*, **91**(12-15), 1613-1625.

Tamura, Y., Kikuchi, H. and Hibi, K. (2007), "Peak normal stresses and effects of wind direction on wind load combinations for medium-rise buildings", *J. Wind Eng. Ind. Aerod.*, **96**(6-7), 1043-1057.

Tamura, Y., Kareem, A., Solari, G., Kwok, K.C.S., Holmes, J.D. and Melbourne, W.H. (2005), "Aspects of the dynamic wind-induced response of structures and codification", *Wind Struct*., **8**(4) 251-268.

Venanzi, I. (2006), "Torsional response of high-rise buildings exposed to turbulent wind", *Proceedings of the 7th UK Conference on Wind Engineering*, Glasgow, 4-6 September.

Wu, J.R. and Li, Q.S. (2008), "Wind-induced lateral-torsional coupled responses of tall buildings", *Wind Struct*., **11**(2), 153-178.

Xie, Z.N. and Gu, M. (2005), "A correlation-based analysis on wind-induced interference effects between two tall buildings", *Wind Struct*., **8**(3), 163-178.

JH